FACULTY OF SCIENCE
UNIVERSITY OF COPENHAGEN, DENMARK
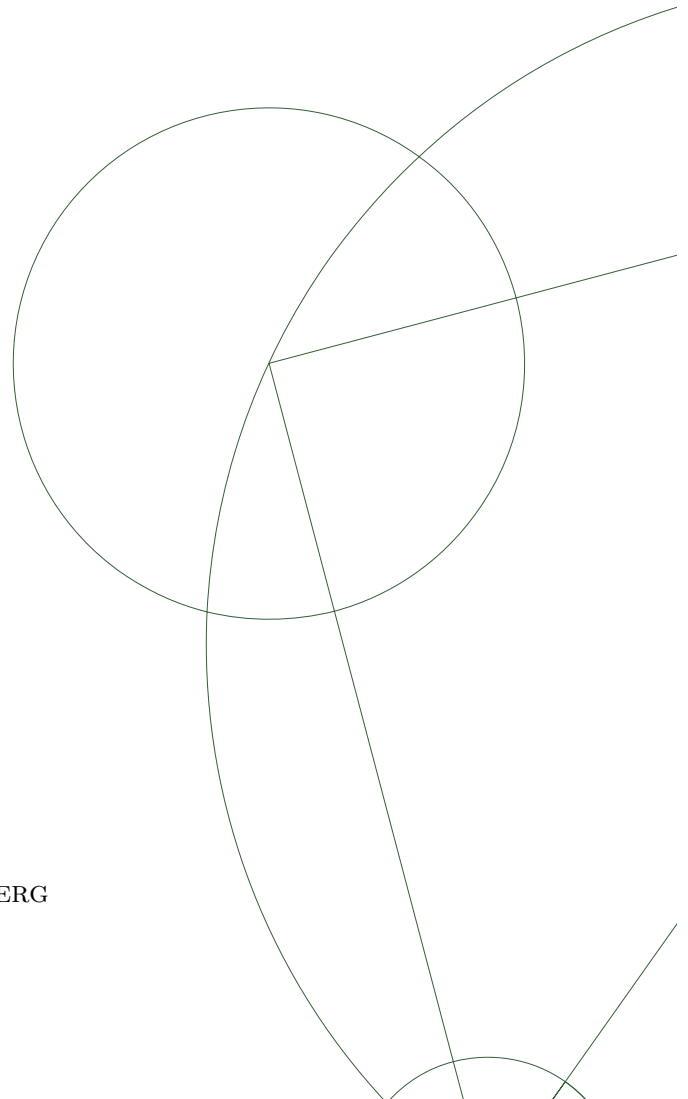
BACHELOR THESIS

MODELLING HEAT CONDUCTION IN ICE SHEETS

OLIVER ACKERMANN LYLLOFF
MAY 27, 2011

SUPERVISORS
ASLAK GRINSTED & CHRISTINE SCHØTT HVIDBERG

Resumé

Borehulstemperaturer og iskernedata fra GRIP er benyttet til at modellere en 112200 år lang temperaturhistorie. En varme- og isflydemodel er blevet udledt og implementeret numerisk ved Crank-Nicolson metoden. Inputparametre til modellen er blevet optimeret, ved inverse analyse, til at give det bedst mulige fit til borehulstemperaturerne fra GRIP. To metoder er blevet testet; en afhængig af isotop sammensætningen af GRIP kernen, mens den anden kun afhænger af tidligere overflade temperaturer. Den første har standard afvigelse $0.3323°C$ fra GRIP borehulstemperaturer, mens den anden har standard afvigelse $0.0182°C$. Temperaturhistorien fra Dahl-Jensen et al. (1998) er blevet diskuteret udfra en sensitivitetsanalyse af de to metoder med tre forskellige diffusivitetskoefficienter.

Abstract

The GRIP ice core data and borehole temperature has been used to model a temperature record spanning the last 112200 years. A heat- and iceflow model has been derived and implemented through a numerical Crank-Nicolson scheme. Inverse analysis has been used to optimize the input parameters of the model, thus obtaining the best possible fit to the GRIP borehole temperatures. Two methods are tested; one dependent on isotopic composition found in the GRIP ice core and the other only on past surface temperatures. The former method has standard deviation $0.3323°C$ from the GRIP borehole temperatures, while the latter has standard deviation $0.0182°C$. A sensitivity analysis of both methods has been carried out, with three different diffusivity coefficients, to discuss the temperature history derived in Dahl-Jensen et al. (1998).

Contents

1 Introduction

The past and future climate seems to be on everyones lips along with an opinion on the ongoing debate of our future with global warming. The studies of ice cores in Greenland are important, because detailed information about our past climate are stored in the glaciers – waiting to be unveiled. Knowledge of past climates can help us understand the effects of future climate changes.

Every year a layer of snow is deposited on top of the Greenland ice sheet. The composition of the ice holds information about the local temperature, gases in the atmosphere, acidity, chemical abundances etc. (Johnsen et al., 1997). Successive accumulation of annual precipitation compress the underlying snow, which is converted into solid ice. A layering is created down through the ice sheet and within each layer is information stored in high temporal resolution (Johnsen et al., 2001).

A deep ice core drill retrieves the ice from the ice sheet. The ice core is about 8 cm in diameter while the drill leaves a borehole of 13 cm in diameter. One such ice core is the GRIP[1]-core. It was recovered in 1992, cut into pieces in half a meter and stored for laboratory analysis. The borehole was filled with a liquid and left undisturbed for 3 years. Measurements of the temperature down through the liquid-filled borehole is used in determination of past temperatures (Dahl-Jensen et al., 1998).

The scope of this study is to retrieve information about past temperatures through inverse analysis using borehole temperatures.

A non-steady state heat- and iceflow model is derived and optimized to fit the borehole temperatures measured at the GRIP-site. The optimized model reveal information about past climates.

Two methods are tested in the optimization process; first isotopic composition of the ice core is used as indirect knowledge (proxy) of past temperatures, following the method in Johnsen et al. (1995); second, independent of proxy data, a fumble-in-the-dark method is used, where qualified guesses of past temperatures are optimized for the best possible fit. The latter method is a simplified version of the inverse Monte Carlo scheme from Dahl-Jensen et al. (1998). The temperature history derived in Dahl-Jensen et al. (1998) is compared to the derived temperature histories from this study.

The sensitivity of the optimized models are tested with several diffusivity coefficients to investigate the effect of the not well determined diffusion process in solid ice (Johnsen et al., 2000)

First, I will present the basics concepts of the physics of glaciers greatly inspired from Cuffey and Paterson (2010). Then I will present the necessary tools in the development of a numerical heat- and iceflow model along with a walkthrough of the model constructed as part of this thesis.

---

[1]Greenland Ice Core Project

2 The physics

In this section are the necessary physics of borehole temperature modelling derived. The result are used in the numerical scheme presented later on.

2.1 Heat- and iceflow

The physics of a glaciers is complex and not fully understood. Approximations and neglections are often necessary to derive a heat- and iceflow equation that fulfill the specific problem to be solved. The general equation of heat- and iceflow is derived in Cuffey and Paterson (2010). It follows from conservation of energy in a deforming medium and Fouriers law of heat conduction, which states that heat flows from regions of higher temperature to regions of lower temperature.

The coordinate system is placed at the base of the glacier with x-axis horizontal and z-axis vertical, positive upward. Conservation of energy

$$\rho \frac{DE}{Dt} = \dot{S}_E - \frac{\partial q_x}{\partial x} - \frac{\partial q_y}{\partial y} - \frac{\partial q_z}{\partial z} \tag{2.1}$$

where $\dot{S}_E$ represent heat produced by ice deformation, firn compaction and refreezing of water. The gradient of the heat fluxes transports heat between regions of different temperature. The significant component of internal energy is thermal, thus

$$\frac{DE}{Dt} = c\frac{DT}{Dt} = \frac{\partial T}{\partial t} + u\frac{\partial T}{\partial x} + v\frac{\partial T}{\partial y} + w\frac{\partial T}{\partial z} \tag{2.2}$$

where u, v and w are ice advection (i.e. transport) velocities. The gradient of the heat flux q is calculated from Fouriers law

$$-\vec{q} = -K\nabla T \tag{2.3}$$

$$-\frac{\partial q}{\partial z} = K\frac{\partial^2 T}{\partial z^2} + \frac{\partial K}{\partial z}\frac{\partial T}{\partial z} \tag{2.4}$$

with thermal conductivity K and similar in the x- and y-direction. The change in thermal conductivity depends on temperature and density and is only significant in the z-direction

$$\frac{dK}{dz} = \frac{\partial K}{\partial \rho}\frac{\partial \rho}{\partial z} + \frac{\partial K}{\partial T}\frac{\partial T}{\partial z} \tag{2.5}$$

Inserting equations (2.2), (2.4) and (2.5) into (2.1) gives the non-steady state heat- and iceflow equation

$$\rho c\frac{\partial T}{\partial t} = K\nabla^2 T - \rho c\left(u\frac{\partial T}{\partial x} + v\frac{\partial T}{\partial y}\right) + \left(\frac{dK}{dz} - \rho cw\right)\frac{\partial T}{\partial z} + \dot{S}_E \tag{2.6}$$

as derived in Cuffey and Paterson (2010).

2.1.1 The simplified equation of heat- and iceflow

In this study a simplified version of (2.6) is used to fit a modelled temperature profile to the borehole temperatures from GRIP. The heat sources in $\dot{S}_E$ are neglected along with advection in x- and y-directions. The density dependence is also neglected in dK/dz (eq. 2.5). This simplifies to,

$$\frac{\partial T}{\partial t} = \frac{K}{\rho c}\frac{\partial^2 T}{\partial z^2} + \left(\frac{1}{\rho c}\frac{dK}{dz} - w\right)\frac{\partial T}{\partial z} \tag{2.7}$$

$$\text{or} \quad \frac{\partial T}{\partial t} = \frac{K}{\rho c}\frac{\partial^2 T}{\partial z^2} - w\frac{\partial T}{\partial z} + \frac{1}{\rho c}\frac{\partial K}{\partial T}\left(\frac{\partial T}{\partial z}\right)^2.$$

The first term on the right hand side of (2.7) is the thermal conductivity from Fouriers law. The coefficient $K/\rho c$ is called the diffusivity $\left[m^2/s\right]$ and is treated in section 2.1.3. The second term of (2.7) relates to iceflow by advection. The horizontal advection is assumed negligible because GRIP is located at an ice divide (Johnsen et al., 1995). In general the horizontal advection is not negligible and should be included in the heat- and iceflow equation.

This simplification applies to the GRIP location according to Johnsen et al. (1995).

2.1.2 Ice flow model

The advection velocity profile used in equation (2.7) is a Dansgaard-Johnsen flow model. It assumes a constant *horizontal* velocity from the surface and down to a specific height h (the kink height), where it decreases linearly to zero at bedrock (Dansgaard and Johnsen, 1969). The model can be modified in several ways, in this study a bottom sliding is added, to allow a non-zero ice-velocity at bedrock. The model depend on accumulation rates λ and the ice thickness H; both of which can be a function of time. In this study only the accumulation rate history changes with time.

As noted in section 2.1.1 only the *vertical* advection velocity is included in the heat- and iceflow equation, so the vertical component of the advection velocity must be calculated. It is assumed that the ice is incompressible and the density is constant. From the continuity equation (in 2D),

$$\frac{\partial \rho}{\partial t} + \rho\left(\frac{\partial w}{\partial z} + \frac{\partial u}{\partial x}\right) = 0 \xRightarrow{\frac{\partial \rho}{\partial t}=0} \tag{2.8}$$

$$\frac{\partial w}{\partial z} + \frac{\partial u}{\partial x} = 0 \tag{2.9}$$

is the vertical component found, here with constant thickness H,

$$w(z) = \frac{\lambda(t)}{H_e} \cdot \begin{cases} z - \frac{h}{2}(1 - f_b), & h \leq z \leq H \\ z f_b + \frac{z^2}{2h}(1 - f_b), & z < h \end{cases} \tag{2.10}$$

4

where $H_e = H - \frac{h}{2}(1 - f_b)$ is the effective height, h is the kink height and f_b is the bottom sliding ratio (Notes on Continuum Mechanics, Dahl-Jensen). The advection velocity as function of depth is plotted in figure 1.
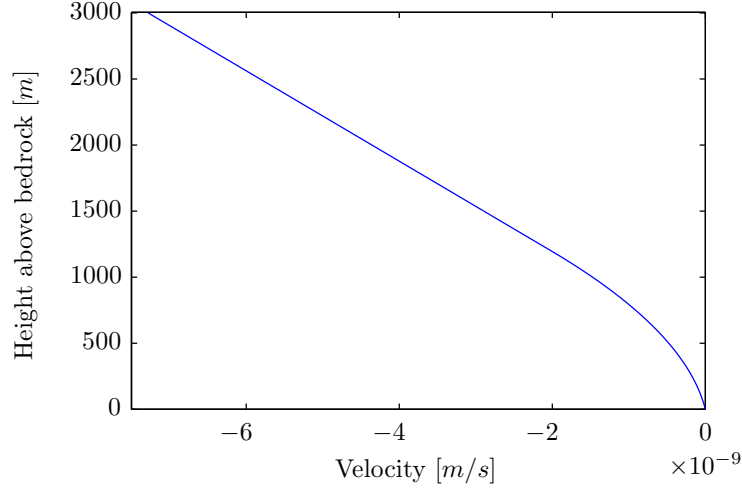

Figure 1: Vertical advection velocity has a linear relationship from the surface and down to the kink height from where it continues as a squared relationship (Dansgaard and Johnsen, 1969).

2.1.3   Thermal properties of ice

Most of the known thermal properties of ice has been found empirically in laboratories. The thermal conductivity depends on density and temperature. It decreases with increasing temperature and increases the increasing density (Cuffey and Paterson, 2010). Different formulae for the thermal parameters are used in the litterature. Thermal conductivity K, specific heat capacity c, density ρ and thermal diffusivity α_T are presented in SI-units, except T which is in °C,

in Cuffey and Paterson (2010):

$$K(T) = 9.828 \exp\left(-5.7 \cdot 10^{-3}(T + 273.15)\right) \tag{2.11}$$

$$K(\rho) = 2.1 \cdot 10^{-2} + 4.2 \cdot 10^{-4}\rho + 2.2 \cdot 10^{-9}\rho^3 \tag{2.12}$$

$$c = 152.5 + 7.122(T + 273.15) \tag{2.13}$$

Fukusako (1990) found

$$K(T) = 1.16\left(1.91 - 8.66 \cdot 10^{-3}T + 2.97 \cdot 10^{-5}T^2\right) \tag{2.14}$$

$$\rho = 917\left(1 - 1.17 \cdot 10^{-4}T\right) \tag{2.15}$$

$$c = 185 + 6.89(T + 273.15) \tag{2.16}$$

James (1968) determined the diffusivity with some discrepancies from ice crystal orientations

$$\alpha_T = (8.43 - 0.101T) \cdot 10^{-7} (-40^\circ C < T < 60^\circ C) \tag{2.17}$$

The diffusivity can be calculated as $K/\rho c \equiv \alpha_T$. This gives 3 different formulae for the diffusivity. The derived diffusivity coefficients are plotted in figure 2.

Diffusivity coefficients can be interpreted as the rate of mobility of temperature in ice. Temperature velocity propagate proportional to the square root of the diffusivity (Cuffey and Paterson, 2010).
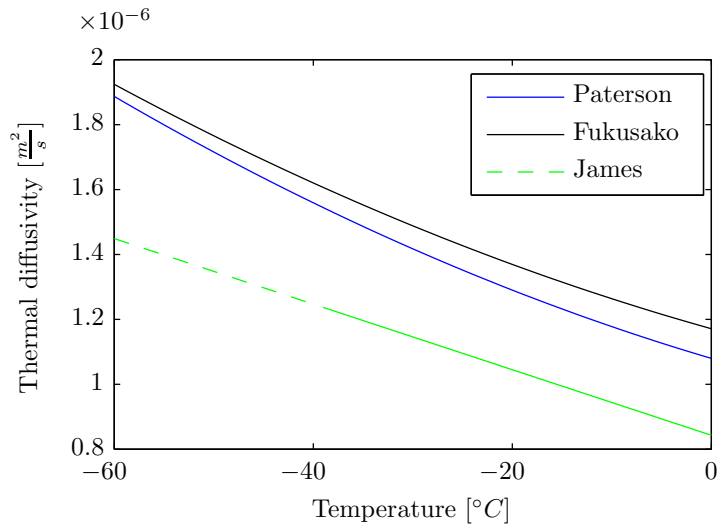

Figure 2: Thermal diffusivity as function of temperature.

2.1.4   Boundary conditions

The heat- and iceflow equation (2.7) can be solved numerically given certain boundary conditions. There are two or three boundary conditions, depending on the specific setup.

The upper boundary condition depends on past surface temperatures (which can be dependent on proxy data). At the surface (ice thickness H),

$$T_{model}(t, z = H) = T_{surf}(t). \tag{2.18}$$

At the bottom of the domain the geothermal heat flux is held constant. This approximation is justified because the temperatures at the base of the GRIP borehole are well below melting point (Cuffey and Paterson, 2010),

$$\left. \frac{\partial T}{\partial z} \right|_{z=0} = -\frac{Q_{geo}}{K}. \tag{2.19}$$

6

In most papers on temperature profiles (e.g. Johnsen et al. 1995; Dahl-Jensen et al. 1998) a slab of rock is included in extent of the bedrock to account for climate-induced temperature changes near bedrock. This calls for a third boundary condition at the interface between ice and rock. The geothermal heat flux changes at the interface because of the difference in conductivity ($\approx 2.1\,\mathrm{W/Km}$ for ice and $2.5\,\mathrm{W/Km}$ for rock). The boundary condition at the interface insures that the heat- and iceflow equation is continuous. The geothermal heat flux in the ice must be equal to the heat flux in the rock.

$$Q_{geo,ice}^{interface} = Q_{geo,rock}^{interface} \tag{2.20}$$

$$-K_{ice}\left.\frac{\partial T}{\partial z}\right|_{z=interface} = -K_{rock}\left.\frac{\partial T}{\partial z}\right|_{z=interface} \tag{2.21}$$

With these boundary conditions a numerical solution to the heat- and iceflow equation (2.7) can be found. The numerical scheme is introduced in section 3 and the numerical version of the boundary conditions can be found in appendix A.

2.2   Isotopic composition of precipitation

When precipitation is forming, temperature exerts a strong influence on the resulting isotopic composition (Johnsen et al., 1995). This concept was first proposed by Willi Dansgaard in 1953 and has numerous applications in the analysis of ice core data.

Isotopic composition is described by *delta notation* and often given in delta values of ‰. The delta notation is calculated from ratios of two measured quantities, R to a standard ratio R_s (e.g Standard Mean Ocean Water),

$$\delta = \left[\frac{R}{R_s} - 1\right] \cdot 10^3\ ‰ \tag{2.22}$$

There are several standard ratios for different isotopes. $R_{SMOW} = [^{18}O]/[^{16}O]$ is widely used in glaciology. In this study, the notation δ refers to the ratio

$$\delta^{18}O = \left[\frac{R}{R_{SMOW}} - 1\right] \cdot 10^3\ ‰. \tag{2.23}$$

where $R = [^{18}O]/[^{16}O]$ measured in the ice core.

Water evaporates from the subtropical ocean and is transported away from the source area. Cooling of the air mass leads to precipitation and the δ-value drops due to preferentially depletion of heavier isotopes (^{18}O). A latitudinal, altitudinal and continental effect is observed with decreasing δ-values towards the poles, higher altitudes and above continents respectively (Dansgaard, 1976). This is the process of *fractionation*.

Seasonal and longterm variations in temperature can be observed in the δ-profile obtained from the ice sheet. Information of high temporal resolution are stored in the ice,

where winter and summer as well as the ice age are visible. The current relationship between surface temperature and δ are known from empirical studies (Johnsen et al., 1995),

$$\delta = 0.67T - 13.7 \text{ ‰} \tag{2.24}$$

and can in general not be used to model past climate.

The key point here is, that the isotopic composition of precipitation (hence snow), gives indirect information about the temperature of which it was formed.

2.2.1 Surface temperature history

The temporal relationship between surface temperature and δ can be found by modelling the measured borehole temperatures to a non-steady state heat- and iceflow equation and calibrating the relationship with a second-order dependency

$$Ts = a + b\delta + c\delta^2 \tag{2.25}$$

e.g. through a least squares fit (Johnsen et al., 1997).

For an optimization method with no δ-dependence, past surface temperatures are pure guess. Former studies can however be used as initial guesses.

2.2.2 Accumulation rates

The accumulation rate history λ has been determined by studying differences in the thickness of annual layers and isotopic composition in the ice core (Dahl-Jensen et al., 1993),

$$\lambda(\delta) = \lambda_0 \exp(-10.09 - 0.653\delta - 0.01042\delta^2) \tag{2.26}$$

from Johnsen et al. (1995), where $\lambda_0 = 0.23 \, \text{m/year}$, is the present day accumulation rate. A depth-age relation for the GRIP ice core can be seen in figure 6 (appendix B).

It can be of interest to know past accumulation rates independent of δ, Dahl-Jensen et al. (1998) gives λ directly from past unknown surface temperatures T_s,

$$\lambda(T) = \lambda_0 \exp\left[0.0467(T_s - T_0) - 0.000227(T_s - T_0)^2\right]. \tag{2.27}$$

where $T_0 = 31.70°C$, the present day surface temperature at the GRIP-site (Dahl-Jensen et al., 1998).

Both accumulation rate histories are used in this study and depends on the optimization method chosen to derive past surface temperatures.

All the necessary physics are now derived and ready to be applied. The tools applying the physics are presented in the next section.

3 The tools

The tools presented in this section has many applications in general. Here they are used to develop and apply the derived physics of section 2.

The output of the heat- and iceflow equation is the temperature as function of depth in the ice sheet for all timesteps. The computation depend on geothermal heat flux, ice flow pattern, surface temperatures and accumulation rates (Johnsen et al., 1995). This is the input, which was covered in section 2. The numerical setup should be formed around the physics and developed for each specific situation.

A part of the numerical setup is choosing a coordinate system, numerical solution scheme, resolution of data and a suitable optimization method for the inverse analysis. These are all important aspects of modelling and a great part of the scope of this thesis.

A full numerical analysis, and the basis of the results presented, involves several steps:

1. Developing a forward model, that can solve the heat- and iceflow equation given certain boundary conditions, surface temperature history, accumulation rate history and respective constants.

2. A loglikelihood function, that measures the misfit between model and data. This involves a covariance matrix with uncertainties.

3. Parameter optimization by maximizing the loglikelihood function.

These steps are presented in the following subsections.

3.1 Forward model

A coordinate system is determined. The origin is placed at the interface between ice and rock with negative z-values below and positive above. A 3km slab of rock is included in the setup. This is done to ensure heat conduction into the bedrock and allows the temperature gradient to vary over time at the interface between ice and rock. The numerical model runs from the bottom $z = -3000m$ to $z = 3003.8 = H$, the height of the GRIP-site (Dansgaard et al., 1993). Since negative integers are not allowed, i, the height step, runs from 0 to $3000m + 3003.8m$ in steps of 5m.

The time starts -112200 years before present (BP) and runs with increasing resolution until present.

$$\texttt{t} = [-112200 : 1000 : -40000, -39000 : 100 : -15000, -14900 : 20 : 0]$$

This makes the computations more efficient and is based on the fact, that resolution decreases with time (Dahl-Jensen et al., 1998).

The simplified heat- and iceflow equation (2.7), must be discretized before it can be solved numerically. A Crank-Nicolson method is chosen to minimize the error, optimize

efficiency and because it is unconditional stable (Recktenwald, 2011). The method can be used to solve non-linear partial differential equations of the form

$$\frac{\partial T}{\partial t} = \frac{\partial^2 T}{\partial z^2} \tag{3.1}$$

which is the one dimensional heat equation.

The derivation of the Crank-Nicolson method and the resulting numerical heat- and iceflow equation can be found in appendix A.

The numerical scheme evolves from an initial temperature profile. The real temperature profile (112200 years ago) is unknown so the present day GRIP profile is used. This can be done, because it is assumed that the initial conditions are forgotten, when the latest 10000 years are generated (Dahl-Jensen et al., 1998).

For the inverse analysis is Matlabs `fminsearch`-function chosen to minimize the (minus)loglikelihood function, which is based on the Nelder-Mead simplex method (Lagarias et al., 1998).

The above derivations and conditions result in a forward model. The derivations are quite tedious, so it is placed in appendix A, the numerical Matlab-code is included in appendix C. The next step, now with the forward model in place, is the loglikelihood function and the basics of inverse analysis.

3.2   Inverse analysis

The objective of almost any scientific experiment is to measure some observed outcome and infer a theory that predicts future outcomes of the same experiment. This is the basics of physical theories and laws. In a more formalized way, we can say that we wish to relate parameters of a model, $\mathbf{m}$ to an observed dataset, $\mathbf{d}$. This relation can be described by the forward operator $\mathbf{G}$

$$\mathbf{G}(\mathbf{m}) = \mathbf{d} \tag{3.2}$$

where $\mathbf{m}$ is an s element vector of model parameters and $\mathbf{d}$ is an r element vector of datapoints (Tarantola, 2005; Aster, 2005).

A forward problem is to find $\mathbf{d}$ given $\mathbf{m}$ (this is analogous to finding datapoints (x, y) of the function $f(x) = ax + b$ where a and b are given).

Tarantola (2005) calls it a 'naïve point of view':

> Taking first a naïve point of view, to solve a *forward problem* means to predict the error-free values of the observable parameters $\mathbf{d}$ that would correspond to a given model $\mathbf{m}$.
>
> *Tarantola (2005).*

The 'naïve' in this viewpoint is to believe in a perfect experiment. All observations contain errors and noise, which can arise from uncertainties in the measurement, numerical round-offs etc. Predicted values can, in general, not be identical to the observed (Tarantola, 2005; Aster, 2005).

The model parameters, and how they relate to observed data, can also hold uncertainties or imperfections. This knowledge is what characterizes an inverse problem. It is to find $\mathbf{m}$ given $\mathbf{d}$,

$$\mathbf{m} = \mathbf{G}^{-1}(\mathbf{d}) \tag{3.3}$$

(or by analogue as above; it is to find parameters a and b that fits $f(x) = ax + b$ to some datapoints (x, y) that might contain some amount of noise).

The prior (a priori) knowledge of a system is used in formulating and solving the inverse problem hence obtaining posterior (a posteriori) knowledge about the model parameters and the relation to observed data. Posterior knowledge can be a likelihood[2] function, which measures how well observed data $\mathbf{d}^{obs}$ fit predicted data $\mathbf{d}^{pre} = \mathbf{G}(\mathbf{m})$. The likelihood, misfit and loglikelihood functions are

$$L(\mathbf{m}) = \exp(-S(\mathbf{m})) \tag{3.4}$$

$$S(\mathbf{m}) = \frac{1}{2}\left(\mathbf{G}(\mathbf{m}) - \mathbf{d}^{obs}\right)^T \mathbf{C}^{-1}\left(\mathbf{G}(\mathbf{m}) - \mathbf{d}^{obs}\right) \tag{3.5}$$

$$\log(L(\mathbf{m})) = l(\mathbf{m}) = -S(\mathbf{m}) \tag{3.6}$$

where $\mathbf{C}$ is the covariance matrix of uncertainties in $\mathbf{d}^{obs}$, which follows a Gaussian distribution (Mosegaard and Tarantola, 1995).

By maximizing the loglikelihood function we get the most *probable* solution to the inverse problem (Aster, 2005).

3.2.1 Covariance matrix

In this study the covariance matrix holds uncertainties in measurements of temperature and depth of the liquid filled borehole. Notes from the logging procedure (Hvidberg et al., 2002) is used in the construction of the covariance matrix.
First Gaussian noise η, is added to the predicted depths[3],

$$\mathbf{z}^{obs} = \mathbf{z}^{pre} + \eta \tag{3.7}$$

The noise added has mean $\mathbf{z}^{pre}$ and standard deviation 0.001m. This estimate fits well with the error noted in Hvidberg et al. (2002). The constructed $\mathbf{z}^{obs}$ are used with the

---

[2]In Sambridge and Mosegaard (2002) it's defined as: *a function describing the probability that a given parameterized model is consistent with observed data.*

[3]The depths are constructed as steps of 5 m, from the base of the ice sheet to the surface

forward model, to interpolate GRIP borehole temperatures resulting in $\mathbf{d}^{obs}$. The misfit between constructed and observed temperatures gives the covariance matrix,

$$S_z = \mathbf{d}^{pre} - \mathbf{d}^{obs} \tag{3.8}$$

$$\mathbf{C}_z = S_z \cdot S_z^T. \tag{3.9}$$

To eliminate bias it is computed from the mean of $N = 800$ $m \times m$ matrices, where m has same dimension as z. The uncertainties in the temperature measurements are ± 5mK (Dahl-Jensen et al., 1998) (independent of depth), which gives a diagonal covariance matrix

$$\mathbf{C}_\sigma = \sigma^2 \cdot \mathbf{I} \tag{3.10}$$

The respective covariance matrices are added together $\mathbf{C} = \mathbf{C}_z + \mathbf{C}_\sigma$.

3.2.2 Estimating confidence intervals

Confidence intervals of each parameter in $\mathbf{m}$ can be approximated by calculating the *observed information matrix* $I_O(\mathbf{m})$ which is minus the Hessian matrix (the second-order partial derivates). The following is adapted from Coles (2001),

$$I_O(\mathbf{m}) = \begin{bmatrix} -\frac{\partial^2 l(\mathbf{m})}{\partial m_1^2} & \cdots & & -\frac{\partial^2 l(\mathbf{m})}{\partial m_1 \partial m_n} \\ \vdots & \ddots & -\frac{\partial^2 l(\mathbf{m})}{\partial m_i \partial m_j} & \vdots \\ & -\frac{\partial^2 l(\mathbf{m})}{\partial m_j \partial m_i} & \ddots & \\ -\frac{\partial^2 l(\mathbf{m})}{\partial m_n \partial m_1} & \cdots & & -\frac{\partial^2 l(\mathbf{m})}{\partial m_n^2} \end{bmatrix} \tag{3.11}$$

here $l(\mathbf{m})$ is the log-likelihood function.

The confidence intervals is derived from the diagonal elements of the inverse $I_O^{-1}(\mathbf{m})_{i,i}$, such that,

$$m_i \pm z_{\frac{\alpha}{2}} \sqrt{I_O^{-1}(\mathbf{m})_{i,i}} \tag{3.12}$$

where $z_{\frac{\alpha}{2}}$ is the $(1 - \frac{\alpha}{2})$ quantile of the standard normal distribution. For the 95% confidence interval it is $\Phi(z) = 1 - \frac{1-0.95}{2} = 0.975 \Rightarrow z_{\frac{\alpha}{2}} = \Phi^{-1}(0.975) = 1.96$.

3.3 Two optimization methods

Past surface temperatures are computed by maximizing the loglikelihood function with respect to the free parameters, that gives the best fit between modelled and measured borehole temperatures from GRIP.

Two methods are applied. In the following denoted method 1 and method 2:

1. Based on the GRIP δ^{18}O-record, this method is similar to the one used in Johnsen et al. (1995). Past surface temperatures and accumulation rates are a function of δ^{18}O. The second order relation (equation 2.25) to the past surface temperatures are unknown and gives 3 free parameters for optimization. The geothermal heat flux is also free to vary, thus giving a total of 4 degrees of freedom.

   Variables assumed constant are bottom sliding ratio $f_b = 0.15$, total height of the ice sheet and the kink height $H = 3003.8$ and $h = 1200$ respectively (Dansgaard et al., 1993). The initial parameters of past surface temperatures are $a = -211, 4°C$, $b = -11.88°C/‰$, $c = -0.1925°C/(‰)^2$. The accumulation rate is a known function of the GRIP δ^{18}O-record (equation 2.26).

2. Based on qualified guesses of the past unknown surface temperatures. This "fumble-in-the-dark" method seek the best fit to the GRIP borehole temperatures, given 10 variable surface temperatures back in time. 10 points in time have been chosen with increasing distance to keep computational run-time down. The default number of function evaluations of `fminsearch` is 200 per parameter. The average run time is 3-5 minutes for optimization of 10 parameters. Initial parameters are adapted directly from Dahl-Jensen et al. (1998) and given in table 1.

   This method holds 11 degrees of freedom in total, 10 from the past unknown surface temperatures and the geothermal heat flux.

   Past accumulation rates are computed from (equation 2.27).

   Variables f_b, H and h are assumed constant as above.

A comparison of the two methods are discussed in section 5.4.

Years BP (kyr)	Temperature $°C$	σ
112.200	-40.000	7.000
25.000	-55.537	5.000
10.000	-34.252	2.000
8.200	-29.974	2.000
7.000	-29.301	2.000
5.000	-29.245	2.000
2.000	-31.907	1.000
1.000	-30.708	1.000
0.400	-32.236	0.500
0.000	-31.710	0.100

Table 1: Surface temperatures from Dahl-Jensen et al. (1998) used as initial guess.

4 Results & analysis

First the physics was derived, then it was converted into a forward model and applied through inverse analysis and here are the results.

Two optimization methods are tested, both of them with three different diffusivity coefficients to investigate the sensitivity of the method and the forward model.

Past surface temperatures computed from the GRIP δ^{18}O-record, following method 1, are plotted in figure 3(a) with corresponding parameters in table 3. In figure 3(b) and table 4 are the results of method 2.

The surface temperature history derived in this study, are best fits to the measured borehole temperatures. Standard deviations are noted in table 2 and deviations as function of depth are plotted in figure 4. The confidence intervals are smaller than four significant digits and not shown in the figures or tables.

The temperature history given in Dahl-Jensen et al. (1998) are used as reference. It has been derived from an inverse Monte Carlo method, where 126 free parameters are optimized, to fit the borehole temperatures from GRIP. The temperature history shown (in red), is the most likely of 2000 models, with standard deviations showing increasing uncertainty back in time (error bars in figure 3(b)). The temperature history provide an excellent fit to the borehole temperatures but cannot be used to date distinct (short-termed) climatic events.

Only the last 10000 years are shown in the figures, because the initial conditions are assumed to be present in the earlier temperature history.

	Method 2	Method 1
Paterson	0.0114	0.3234
Fukusako	0.0088	0.4256
James	0.0344	0.2480
$\langle\texttt{std}\rangle$	0.0182	0.3323

Table 2: Standard deviations for the two methods and for each diffusivity coefficient.

	a	b	c	Q_{geo}
Paterson	-11.451	-1.634	-0.063	0.057
Fukusako	-9.008	-1.534	-0.062	0.058
James	-60.134	-3.247	-0.069	0.051

Table 3: Derived parameters from method 1.

	Paterson	**Fukusako**	**James**
$T_s(t_1)$	-35.3923	-39.3486	-28.1909
$T_s(t_2)$	-58.9432	-57.4783	-45.6422
$T_s(t_3)$	-35.1083	-36.1020	-33.0400
$T_s(t_4)$	-30.4940	-29.9417	-31.3205
$T_s(t_5)$	-29.5523	-28.7600	-32.1921
$T_s(t_6)$	-30.2102	-30.2249	-30.7716
$T_s(t_7)$	-31.3780	-31.3824	-31.0461
$T_s(t_8)$	-31.0237	-30.9474	-31.4373
$T_s(t_9)$	-32.2939	-32.3481	-32.1350
$T_s(t_{10})$	-31.6531	-31.6203	-31.7033
Q_{geo} $[W/Km]$	0.0500	0.0504	0.0499

Table 4: Derived surface temperatures from method 2. $T_s(t_1)$ refers to the surface temperature at $t_1 = 112$kyr BP following the years in table 1.
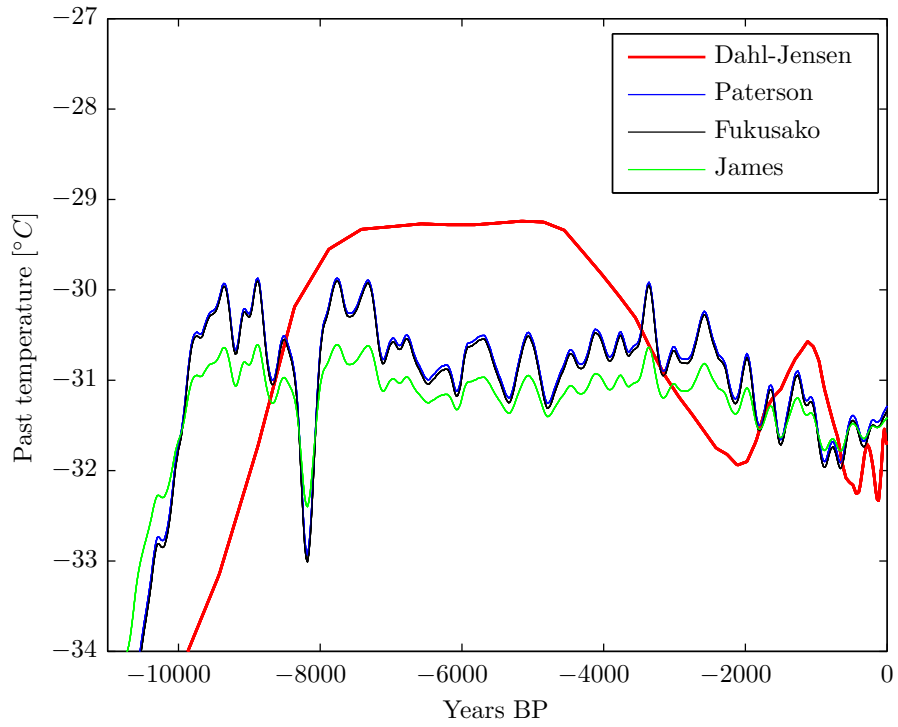
(a) Method 1, past surface temperatures derived from the δ^{18}O-record. Dahl-Jensen et al. (1998) temperature history are plotted as reference.
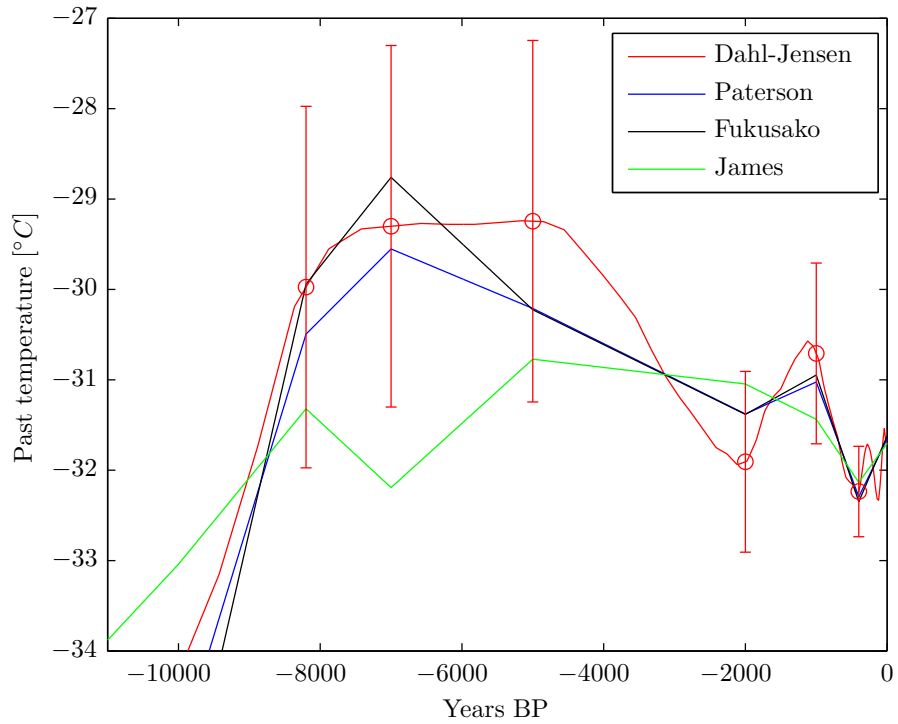
(b) Method 2, past surface temperatures derived from "fumble-in-the-dark". Solid lines connect the optimized parameters. Dahl-Jensen et al. (1998) temperature history are plotted as reference.

Figure 3: Past surface temperatures derived from (a) method 1, filtered with a 200-year Gaussian low-pass filter; (b) method 2.
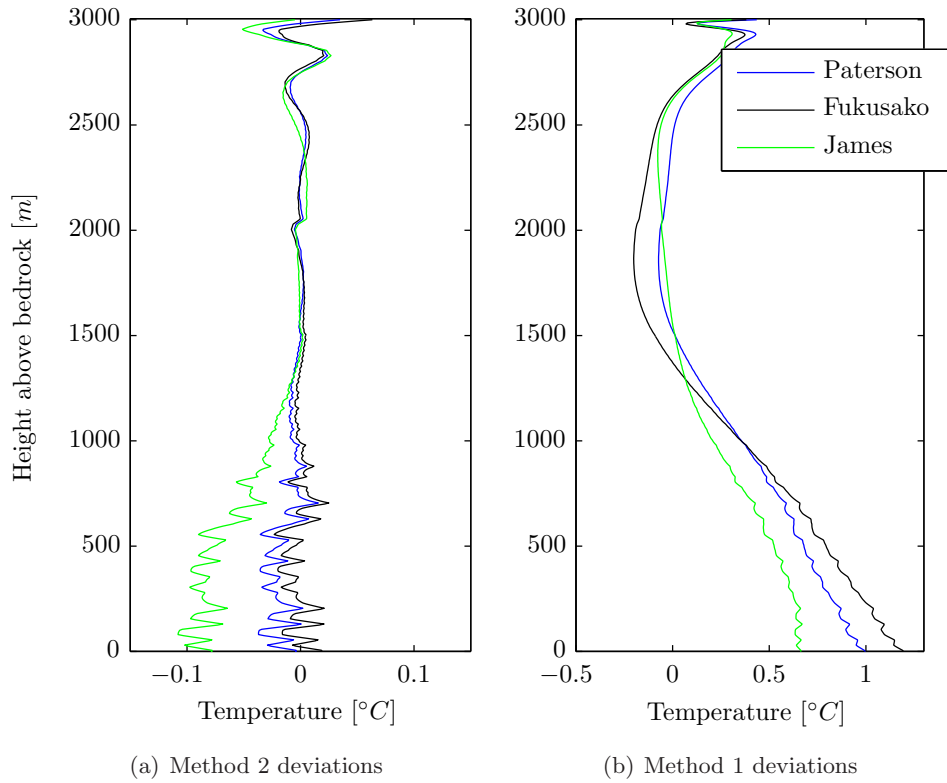
(a) Method 2 deviations (b) Method 1 deviations

Figure 4: Deviations from GRIP borehole temperatures as function of depth for the two methods. The fluctuations near the bottom arise from decreasing resolution back in time.

5 Discussion

The results derived from the δ^{18}O-record (method 1) and past unknown surface temperatures (method 2) are discussed in the following sections. A comparison of the two methods follows along with a discussion of the diffusivity coefficients.

5.1 Temperature history – method 1

The surface temperatures derived from method 1, has an average standard deviation of $\langle\sigma\rangle = 0.3323°C$ from the GRIP borehole temperatures.

Deviations as function of depth are plotted in figure 4(b). The fit is best from a depth of 500m to 1500m. Increasing deviations are seen from a depth of 1500m to bedrock. This misfit is also observed in the temperature history derived via method 2 (figure 4(a)), though somewhat smaller, section 5.4 has a discussion on this.

Some features can be observed in the figure; a rapid increase in temperature up to 10000 years BP marking the start of Holocene (our present interglacial period); a short and rapid decrease in surface temperature at 8.2 kyr BP (the 8.2 kyr event). More subjective observations, include a post-glacial climatic optimum lasting from 10 kyr to 7 kyr BP, a small decrease in temperature from around 3.5 kyr to 1000 yr BP and a small increase from 1000 yr BP to present.

The derived surface temperature history has few similarities with the history from Dahl-Jensen et al. (1998). An important note in this respect, is that the δ^{18}O-record is also lacking these features, most noticeable is the lack of a Climatic Optimum (CO from 8kyr to 5 kyr BP). Figure 7 in appendix B has plots of the δ^{18}O-record.

The NorthGRIP[4] δ^{18}O-record has a larger shift than the GRIP record during the CO (Johnsen et al., 2001). There are several explanations for this; Johnsen et al. (2001) suggest that precipitation cyclones had easier access to higher latitudes (hence North-GRIP). Another explanation, not just related to the CO, is presented by Vinther et al. (2009). The paper suggest that ice sheet elevation changes are the cause of the flat profile obtained from the GRIP δ^{18}O-record. The elevation changes are derived from gas content of the ice core. The results show that the elevation of the GRIP site was 100-150 m higher 10000 years BP and has decreased steadily to the present height. A rough linear approximation gives a decrease of $150m/10000yr = 0.015\,\mathrm{m}/\mathrm{yr}$.

Vinther et al. (2009) conclude that a correction to the GRIP δ^{18}O-record with respect to elevation changes is necessary to "rehabilitate" δ^{18}O as a reliable temperature proxy.

This is a plausible explanation for the surface temperature history seen in figure 3(a). Elevation changes has counteracted the δ^{18}O signal and evened it out so the CO is not observed.

[4]North Greenland Ice Core Project (Dahl-Jensen et al., 2002).

The sensitivity of the model with respect to the diffusivity coefficient is easily seen. The three diffusivity coefficients show similar results, though the James (1968) gives a lower temperature in general and has a smaller amplitude.

5.2   Temperature history – method 2

The past surface temperatures derived from method 2 has an excellent fit, with $\langle \sigma \rangle = 0.0182°C$. The deviations as function of depth can be seen in figure 4(a).

This is expected because the free parameters, in this method, are independent of each other and can thus provide a better fit.

There are signification differences between the three diffusivity coefficients used. Diffusivities from Cuffey and Paterson (2010) and Fukusako (1990) show similar results with the latter a bit higher at 7 kyr BP. The third diffusivity from James (1968) shows lower temperatures from 7 kyr to 4 kyr BP.

The temperature history derived in Dahl-Jensen et al. (1998) has a noticeable feature from 2000 yr BP to 400 yr BP – the medieval warming that is not seen on the temperatures derived from the GRIP δ^{18}O-record. This warmer period is important for those debating the 'Hockey Stick" controversy (Hockey stick controversy, Wikipedia, 2011). It is out of the scope of this study to go into this debate, but it does however lead to a relevant question: "What is the effect of the diffusivity coefficient on the derived surface temperatures, and can it verify the Dahl-Jensen et al. (1998) temperature history?".

With diffusivities from Cuffey and Paterson (2010) and Fukusako (1990) a small increase in temperature is observed from 2000 yr to 1000 yr BP followed by a rapid decrease to 400 yr BP. All derived surface temperatures are within the standard deviations noted in Dahl-Jensen et al. (1998), except the diffusivity from James (1968) which fall out of the standard deviations at 7 kyr BP, with a temperature profile evolving opposite of the two other diffusivities. This is discussed in the next section.

5.3   The effect of diffusivity

It is evident from figure 3 that a change in the diffusivity coefficient changes the derived surface temperatures. To see if this change is reasonable within what is expected from the physics, a plot of constant diffusivity coefficients are presented in figure 5. Applied to the forward model, it shows that a low diffusivity coefficient gives colder profiles than profiles with higher diffusivity coefficients. This is not a general observation, but an effect of the temperature history at GRIP. What is seen in the figure is actually the amount of temperature-remnants of the last ice age. As mentioned in section 2.1.3, the diffusivity coefficient carries information about the propagation velocity of surface temperatures. The temperature profile with the lowest diffusivity coefficient (far left on figure 5) has the lowest temperature propagation velocity down through the ice sheet, thus making

the the ice age temperatures visible at 1000 m above bedrock. The temperature profile with the highest diffusivity coefficient (far right on the figure) has "forgotten" the ice age because the temperature propagation velocity is much higher.

The three diffusivity coefficients are approximately (1.2, 1.5 and 1.6) $\cdot 10^{-6} m^2/s$ at $T = -30°C$, James (1968), Cuffey and Paterson (2010) and Fukusako (1990) respectively. This correspond to the second, fifth and sixth line from the left on the figure.

The results of method 1 and 2 can be explained from this. The model is evaluated from 112200 years BP up to present. The initial temperature profile is assumed to be forgotten in the derived temperature history, but in the light of the velocity interpretation of diffusivity, it is possible that the initial temperature profile has not been totally forgotten – especially for the James (1968) diffusivity coefficient.

Dahl-Jensen et al. (1998) has a time series starting at 450.000 years BP, more than twice the time scale for thermal equilibrium of ice to bedrock, to ensure that the initial unknown conditions are forgotten, when the latest 50000 years are generated. With a timescale of 112200 years in this study, it is possible that the initial conditions are still present in the ice. And following the calculation from Dahl-Jensen et al. (1998), with a timescale of 112200 years, only about the latest 10000 years, should have forgotten the initial conditions.

5.4 Two methods – a summary

A recap of the observations from the previous subsections show,

1. A better fit with method 2, where past surface temperatures are derived independent of the δ^{18}O-record. The independent parameters are the most likely reason for the good fit.

2. The bigger misfit in method 1, is likely due to parameter-dependence. More parameters could provide a better fit. There are eight degrees of freedom in the analysis of Johnsen et al. (1995), but only 4 is noted specifically, so it has not been possible to reproduce in full. They get a standard deviation of $0.036°C$, about 10 times lower than this study, which implies that the last 4 parameters are crucial for obtaining a better fit.

3. A possible explanation for the flat δ^{18}O-record is an even-out effect from elevation changes at GRIP.

4. Changes in diffusivity coefficients has only little effect on derived surface temperatures and fit within the uncertainties of Dahl-Jensen et al. (1998).

5. Misfits in figure 4 show the biggest discrepancies at the top and bottom of the ice. These misfits are probably a result of the simplifications made to the heat- and iceflow equation and the constants used, e.g. the bottom sliding ratio, the kink
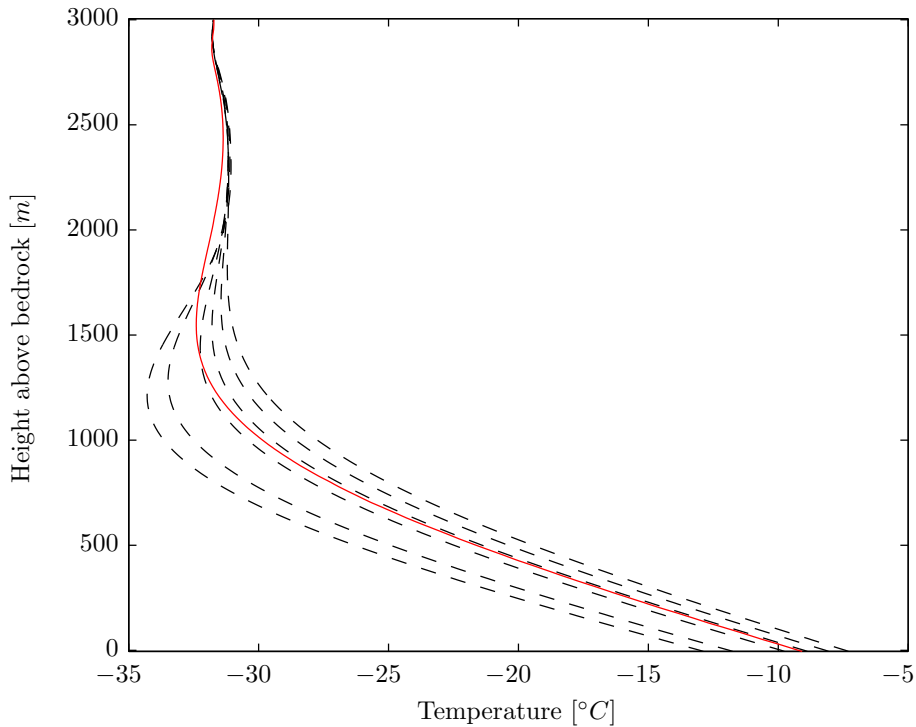
Figure 5: Effect of the diffusivity coefficient on the model. From left to right $\alpha = [1.1, 1.2, \ldots, 1.6] \cdot 10^{-6} [m^2/s]$. Method from (Dahl-Jensen et al., 1998)

height and total height. These constants could be added as input parameters in both methods to give a better fit.

6. The δ^{18}O-record goes 112200 years back, which put a constraint on the timescale in method 1. Method 2 however, is independent of the δ^{18}O-record so the timescale can be chosen freely. This could give a more correct profile near bedrock for the James (1968) diffusivity coefficient.

With a correction of the δ^{18}O-record for elevation changes, suggested by Vinther et al. (2009), could method 1 be able to show high resolution climate changes that method 2 (and Dahl-Jensen et al. (1998)) could not. This could boost the reliability of the method and give more detailed information about past climates.

6   Conclusion

The process of obtaining information about past climates from borehole temperatures has been described in this thesis. The relevant physics has been derived and applied through a numerical forward model. The surface temperature history has been generated via inverse analysis of the borehole temperatures from GRIP. Two methods of parameter optimization has been derived and compared to the temperature history generated in Dahl-Jensen et al. (1998).

Standard deviations of $0.3323^\circ C$ and $0.0182^\circ C$, method 1 and 2 respectively, from the measured borehole temperature, reveal the obvious difference in initial conditions: mutual parameter dependence.

A sensitivity analysis of the methods with respect to three diffusivity coefficients has shown expected results from the discussion on diffusivity. The diffusivity coefficients fit well within the standard deviations of the Dahl-Jensen et al. (1998) temperature history, except the James (1968) diffusivity at 7000 years BP which is $3^\circ C$ colder than Dahl-Jensen et al. (1998). More work needs to be done i order to fully explain the deviation, a starting point would be to increase the timescale, to see if the initial conditions are still present.

The work by Vinther et al. (2009) show how to rehabilitate the δ^{18}O-record. This new record could easily be inferred in the inverse analysis applied in this thesis.

To go into more work on the diffusivity coefficients, a paper by Pettit et al. (2007) show that the flow pattern is affected by crystal orientations of the ice. The effect is most pronounced in the lower half of the ice sheet. This depth-dependency could be used with the James (1968) diffusivity coefficient to search for a better fit.

And a last suggestion would be to turn op the number of parameters in method 2, to get an analysis more like the inverse Monte Carlo used in Dahl-Jensen et al. (1998) and apply the three diffusivity coefficients.

References

Aster, R. C. (2005). *Parameter estimation and inverse problems*. Amsterdam: Elsevier.

Coles, S. G. (2001). *An Introduction to Statistical Modeling of Extreme Values*. Springer Series in Statistics. Springer.

Cuffey, K. and W. S. B. Paterson (2010). *The physics of glaciers*. Amsterdam: Butterworth-Heinemann/Elsevier.

Dahl-Jensen, D. Continuum mechanics. Lecture notes.

Dahl-Jensen, D., N. S. Gundestrup, H. Miller, O. Watanabe, S. J. Johnsen, J. P. Steffensen, H. B. Clausen, A. Svensson, and L. B. Larsen (1 January 2002). The northgrip deep drilling programme. *Annals of Glaciology 35*, 1–4(4).

Dahl-Jensen, D., S. Johnsen, C. Hammer, H. Clausen, and J. Jouzel (1993). Past accumulation rates derived from observed annual layers in the grip ice core from summit, central greenland. In *Ice in the Climate System*, Peltier, W.R., ed., pp. 517–532. Berlin Heidelberg: Springer-Verlag.

Dahl-Jensen, D., K. Mosegaard, N. Gundestrup, G. Clow, S. Johnsen, A. Hansen, and N. Balling (1998, OCT 9). Past temperatures directly from the Greenland Ice Sheet. *Science 282*(5387), 268–271.

Dansgaard, W. (1976). Uddrag af kompendium om glaciologi. Noter om isotopglaciologi.

Dansgaard, W. and S. J. Johnsen (1969, June). A flow model and a time scale for the ice core from Camp Century, Greenland. *Journal of Glaciology 8*, 215–223.

Dansgaard, W., S. J. Johnsen, H. B. Clausen, D. Dahl-Jensen, N. S. Gundestrup, C. U. Hammer, C. S. Hvidberg, J. P. Steffensen, A. E. Sveinbjornsdottir, J. Jouzel, and G. Bond (1993, 07). Evidence for general instability of past climate from a 250-kyr ice-core record. *Nature 364*(6434), 218–220.

Fukusako, S. (1990, MAR). Thermophysical properties of ice, snow, and sea ice. *International journal of thermodynamics 11*(2), 353–372.

Hockey stick controversy, Wikipedia (2011). Hockey stick controversy. `http://en.wikipedia.org/wiki/Hockey_stick_controversy`. Date retrieved: May 22, 2011.

Hvidberg, C., J. Steffensen, H. Clausen, H. Shoji, and J. Kipfstuhl (2002). The NorthGRIP ice-core logging procedure: description and evaluation. Volume 35 of *Annals of Glaciology*, pp. 5–8.

James, D. (1968). The thermal diffusivity of ice and water between-40 and+60 degrees c. *Journal of Materials Science 3*(5), 540–543.

Johnsen, S., H. Clausen, W. Dansgaard, N. Gundestrup, C. Hammer, U. Andersen, K. Andersen, C. Hvidberg, D. DahlJensen, J. Steffensen, H. Shoji, A. Sveinbjornsdottir, J. White, J. Jouzel, and D. Fisher (1997, NOV 30). The delta O-18 record along the Greenland Ice Core Project deep ice core and the problem of possible Eemian climatic instability. *Journal of geophysical reasearch-oceans 102*(C12), 26397–26410.

Johnsen, S., H. Clausen, K. Duffey, G. Hoffmann, J. Schwander, and Cryts (2000). Diffusion of stable isotopes in polar firn and ice: the isotope effect in firn diffusion. In *Physics of ice core records*, pp. 121–140. Hokkaido University Press, Sapporo.

Johnsen, S., D. DahlJensen, N. Gundestrup, J. Steffensen, H. Clausen, H. Miller, V. Masson-Delmotte, A. Sveinbjornsdottir, and J. White (2001, MAY). Oxygen isotope and palaeotemperature records from six Greenland ice-core stations: Camp Century, Dye-3, GRIP, GISP2, Renland and NorthGRIP. *Journal of Quaternary Science 16*(4), 299–307.

REFERENCES

Johnsen, S. J., D. Dahl-Jensen, W. Dansgaard, and N. Gundestrup (1995). Greenland palaeotemperatures derived from grip bore hole temperature and ice core isotope profiles. *Tellus B 47*(5), 624–629.

Lagarias, J. C., J. A. Reeds, M. H. Wright, and P. E. Wright (1998). Convergence properties of the Nelder-Mead simplex method in low dimensions. *SIAM Journal of Optimization 9*, 112–147.

Mosegaard, K. and A. Tarantola (1995, JUL 10). Monte-Carlo sampling of solutions to inverse problems. *Journal of geophysical reasearch-solid earth 100*(B7), 12431–12447.

Pettit, E. C., T. Thorsteinsson, H. P. Jacobson, and E. D. Waddington (2007). The role of crystal fabric in flow near an ice divide. *Journal of Glaciology 53*(181), 277–288.

Recktenwald, G. W. (2011, Mar). Finite-difference approximations to the heat equation. `http://web.cecs.pdx.edu/~gerry/class/ME448/codes/FDheat.pdf`. Date retrieved: May 19, 2011.

Sambridge, M. and K. Mosegaard (2002, DEC 5). Monte Carlo methods in geophysical inverse problems. *Reviews of Geophysics 40*(3).

Tarantola, A. (2005). *Inverse Problem Theory*. Siam.

Tridiagonal matrix algorithm, Wikipedia (2011). Tridiagonal matrix algorithm. `http://en.wikipedia.org/wiki/Tridiagonal_matrix_algorithm`. Date retrieved: May 22, 2011.

Vinther, B. M., S. L. Buchardt, H. B. Clausen, D. Dahl-Jensen, S. J. Johnsen, D. A. Fisher, R. M. Koerner, D. Raynaud, V. Lipenkov, K. K. Andersen, T. Blunier, S. O. Rasmussen, J. P. Steffensen, and A. M. Svensson (2009, 09). Holocene thinning of the greenland ice sheet. *Nature 461*(7262), 385–388.

A The numerical scheme

Many differential equations need to be discretized before they can be solved numerically. The key to this process is Taylor expansions and finite difference approximations. Four difference approximations are used to discretize the differential equation in this study.The following is adapted directly from Recktenwald (2011), $\mathcal{O}$ denotes the order of the truncation error. First the *forward difference* approximation,

$$\left.\frac{\partial \phi}{\partial x}\right|_{x_i} = \frac{\phi_{i+1} - \phi_i}{\Delta x} + \mathcal{O}(\Delta x) \tag{A.1}$$

Similarly by a Taylor series expansion about $\delta x = -\Delta x$ the *backward difference* approximation can be shown to be

$$\left.\frac{\partial \phi}{\partial x}\right|_{x_i} = \frac{\phi_i - \phi_{i-1}}{\Delta x} + \mathcal{O}(\Delta x) \tag{A.2}$$

The *central difference approximation* can be constructed from the two equations above

$$\left.\frac{\partial \phi}{\partial x}\right|_{x_i} = \frac{\phi_{i+1} - \phi_{i-1}}{2\Delta x} + \mathcal{O}(\Delta x^2) \tag{A.3}$$

The *second order central difference approximation* is

$$\left.\frac{\partial^2 \phi}{\partial x^2}\right|_{x_i} = \frac{\phi_{i+1} - 2\phi_i + \phi_{i-1}}{\Delta x^2} + \mathcal{O}(\Delta x^2). \tag{A.4}$$

Tnd the Crank-Nicolson is the average of the central difference approximation and is chosen over e.g. a forward scheme, because of the higher order truncation error $\mathcal{O}(\Delta t^2) + \mathcal{O}(\Delta x^2)$ (Recktenwald, 2011).

The Crank-Nicolson method sets up a system of equations that is solved at each (discrete) time step Δt for all steps in space Δz. The notation for the temperature at time j at height i is T_i^j, hence $t = j \cdot \Delta t$ and $z = i \cdot \Delta z$.

The coordinate system is placed at the bottom of the domain so the z-axis is positive upward. Time runs from -112200 years BP to present with increasing resolution.

The left-hand side of equation (2.7) is approximated by a forward difference in time:

$$\frac{\partial T}{\partial t} \approx \frac{T_i^{j+1} - T_i^j}{\Delta t} \tag{A.5}$$

The first term of the right-hand side of equation (2.7) is approximated with the average of the second order central differences in space (this is special for Crank-Nicolson) and forward difference in time.

$$\alpha_T \frac{\partial^2 T}{\partial z^2} \approx \frac{\alpha_T}{2} \left(\frac{T_{i+1}^{j+1} - 2T_i^{j+1} + T_{i-1}^{j+1}}{(\Delta z)^2} + \frac{T_{i+1}^j - 2T_i^j + T_{i-1}^j}{(\Delta z)^2} \right) \tag{A.6}$$

The second term of the right-hand side of equation (2.7) is approximated with the average of the *first* order central differences in space and forward difference in time.

$$\left(\frac{1}{\rho c}\frac{dK}{dz} - w\right)\frac{\partial T}{\partial z} \approx \frac{(K_\circ - w)}{2}\left(\frac{T_{i+1}^{j+1} - T_{i-1}^{j+1}}{2\Delta z} + \frac{T_{i+1}^{j} - T_{i-1}^{j}}{2\Delta z}\right) \tag{A.7}$$

Where $K_\circ \equiv \frac{1}{\rho c}\frac{dK}{dz}$.

Collecting the above equations gives equation (2.7) in discrete form:

$$\frac{T_i^{j+1} - T_i^{j}}{\Delta t} = \frac{\alpha_T}{2}\left(\frac{T_{i+1}^{j+1} - 2T_i^{j+1} + T_{i-1}^{j+1}}{(\Delta z)^2} + \frac{T_{i+1}^{j} - 2T_i^{j} + T_{i-1}^{j}}{(\Delta z)^2}\right)$$
$$+ \frac{(K_\circ - w)}{2}\left(\frac{T_{i+1}^{j+1} - T_{i-1}^{j+1}}{2\Delta z} + \frac{T_{i+1}^{j} - T_{i-1}^{j}}{2\Delta z}\right) \tag{A.8}$$

Equation (A.8) must be rearranged to set up the system of equations to be solved. All $(j+1)$-terms is collected on the left-hand side and (j)-terms on the right-hand side.

$$T_i^{j+1} - \frac{(K_\circ - w)}{4\Delta z}\Delta t\left(T_{i+1}^{j+1} - T_{i-1}^{j+1}\right) - \frac{\alpha_T}{2\Delta z^2}\Delta t\left(T_{i+1}^{j+1} - 2T_i^{j+1} + T_{i-1}^{j+1}\right) = \tag{A.9}$$

$$T_i^{j} + \frac{(K_\circ - w)}{4\Delta z}\Delta t\left(T_{i+1}^{j} - T_{i-1}^{j}\right) + \frac{\alpha_T}{2\Delta z^2}\Delta t\left(T_{i+1}^{j} - 2T_i^{j} + T_{i-1}^{j}\right) \tag{A.10}$$

By denoting $s_i = \frac{\alpha_T}{2\Delta z^2}\Delta t$ and $r_i = \frac{K_\circ - w}{4\Delta z}\Delta t$,

$$T_i^{j+1} - r_i T_{i+1}^{j+1} + r_i T_{i-1}^{j+1} - s_i T_{i+1}^{j+1} + 2s_i T_i^{j+1} - s_i T_{i-1}^{j+1} = \tag{A.11}$$

$$T_i^{j} + r_i T_{i+1}^{j} - r_i T_{i-1}^{j} + s_i T_{i+1}^{j} - 2s_i T_i^{j} + s_i T_{i-1}^{j} \Leftrightarrow \tag{A.12}$$

$$T_{i+1}^{j+1}(-r_i - s_i) + T_i^{j+1}(1 + 2s_i) + T_{i-1}^{j+1}(r_i - s_i) = \tag{A.13}$$

$$T_{i+1}^{j}(r_i + s_i) + T_i^{j}(1 - 2s_i) + T_{i-1}^{j}(s_i - r_i) \tag{A.14}$$

this tridiagonal system of equations can be written in short

$$a_i T_{i-1}^{j+1} + b_i T_i^{j+1} + c_i T_{i+1}^{j+1} = -a_i T_{i-1}^{j} + b_i^\dagger T_i^{j} - c_i T_{i+1}^{j} \tag{A.15}$$

for $1 < j < n$ with $a_i = (r_i - s_i)$, $b_i = (1 + 2s_i)$, $b_i^\dagger = (1 - 2s_i)$ and $c_i = (-r_i - s_i)$.

In matrix notation $AT^{j+1} = BT^j$

$$\begin{bmatrix} b_1 & c_1 & 0 & \cdots & 0 \\ a_2 & b_2 & c_2 & \cdots & 0 \\ 0 & a_3 & b_3 & \ddots & \vdots \\ 0 & 0 & \ddots & \ddots & c_{n-1} \\ 0 & 0 & \cdots & a_n & b_n \end{bmatrix}\begin{bmatrix} T_1^{j+1} \\ T_2^{j+1} \\ T_3^{j+1} \\ \vdots \\ T_n^{j+1} \end{bmatrix} = \begin{bmatrix} b_1^\dagger & -c_1 & 0 & \cdots & 0 \\ -a_2 & b_2^\dagger & -c_2 & \cdots & 0 \\ 0 & -a^3 & b_3^\dagger & \ddots & \vdots \\ 0 & 0 & \ddots & \ddots & -c_{n-1} \\ 0 & 0 & \cdots & -a_n & b_n^\dagger \end{bmatrix}\begin{bmatrix} T_1^{j} \\ T_2^{j} \\ T_3^{j} \\ \vdots \\ T_n^{j} \end{bmatrix} \tag{A.16}$$

This system can be solved very efficiently with the Thomas Algorithm (Tridiagonal matrix algorithm, Wikipedia, 2011) which is implemented with the user-created Matlab function `TDMAsolver` (see appendix C).

The derivative of the conductivity $K_\circ \equiv \frac{1}{\rho c}\frac{dK}{dz}$ is computed by a difference approximation

$$\frac{dK}{dz} = \frac{\partial K}{\partial T}\frac{\partial T}{\partial z} \approx \tag{A.17}$$

$$\frac{dK}{dz}(i) = -5.7 \cdot 10^{-3} \cdot 9.828 \exp\left(-5.7 \cdot 10^{-3}(T + 273.15)\right)\left(\frac{T_{i+1}^j - T_{i-1}^j}{2z}\right) \tag{A.18}$$

where the conductivity from equation (2.11) are used.

Boundary conditions The tridiagonal system of equations above can be solved with appropriate boundary conditions. The theoretical boundary conditions formulated in section 2.1.4 is adapted to fit the numerical scheme.

At the surface the temperature T_{surf} is determined as a function of time, and the derivation depend on the method chosen. The boundary condition formulated in equation (2.18) is inferred by putting $a_n = 0$, $b_n = 1$ and $d_n = T_{surf}$ in the bottom equation of the tridiagonal matrix:

$$a_n T_{n-1}^{j+1} + b_n T_n^{j+1} = -a_n T_{n-1}^j + b_n^\dagger T_n^j = d_n \tag{A.19}$$

$$T_n^{j+1} = d_n = T_{surf} \tag{A.20}$$

The thermal conductivity changes at the interface between ice and bedrock ($z = z_0$) so the boundary condition formulated in equation (2.21) gives

$$-K_{ice}\frac{\partial T}{\partial z} = -K_{rock}\frac{\partial T}{\partial z} \tag{A.21}$$

$$-K_{ice}\frac{T_{z_0+1}^{j+1} - T_{z_0}^{j+1}}{\Delta z} = -K_{rock}\frac{T_{z_0}^{j+1} - T_{z_0-1}^{j+1}}{\Delta z} \tag{A.22}$$

$$(K_{ice} + K_{rock})T_{z_0}^{j+1} = K_{ice}T_{z_0+1}^{j+1} + K_{rock}T_{z_0-1}^{j+1} \tag{A.23}$$

$$-\frac{K_{ice}}{(K_{ice} + K_{rock})}T_{z_0+1}^{j+1} + T_{z_0}^{j+1} - \frac{K_{rock}}{(K_{ice} + K_{rock})}T_{z_0-1}^{j+1} = 0 \tag{A.24}$$

This is inferred by putting $a_{z_0} = -\frac{K_{rock}}{(K_{ice}+K_{rock})}$, $b_{z_0} = 1$, $c_{z_0} = -\frac{K_{ice}}{(K_{ice}+K_{rock})}$ and $d_{z_0} = 0$.

At the bottom of the bedrock the heat flux is held constant, equation (2.19) gives

$$Q_{geo} = -K_{rock}\frac{\partial T}{\partial z} \approx -K_{rock}\frac{T_2^{j+1} - T_1^{j+1}}{\Delta z} \tag{A.25}$$

$$-\frac{Q_{geo}}{K_{rock}}\Delta z = T_2^{j+1} - T_1^{j+1} \tag{A.26}$$

This is inferred by putting $b_1 = -1$, $c_1 = 1$ and $d_1 = -\frac{Q_{geo}}{K_{rock}}\Delta z$.

27

B   Graphics
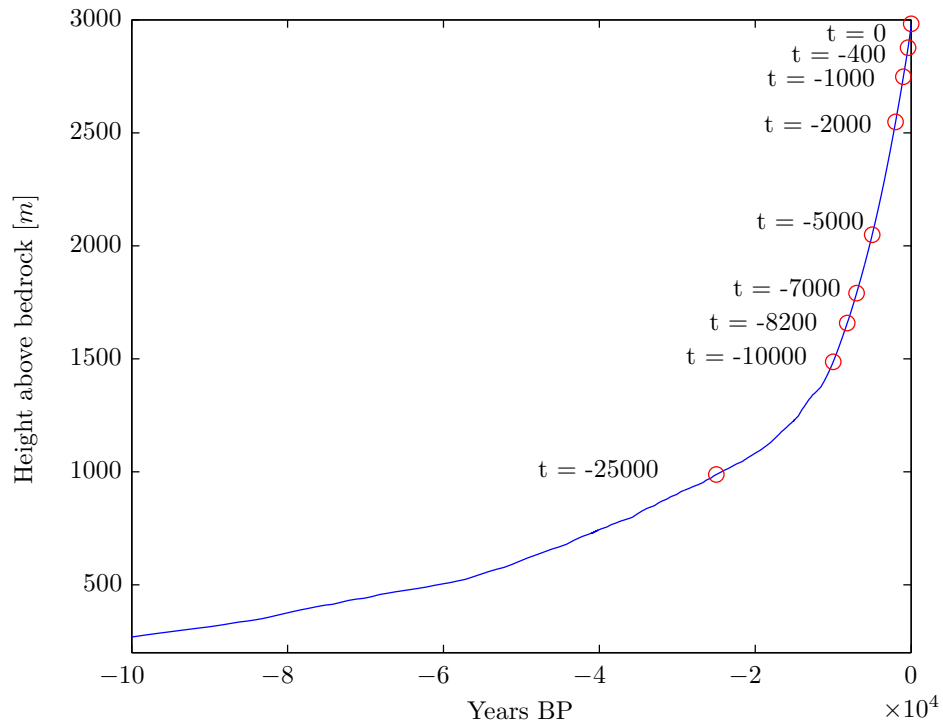

Figure 6: Depth-age relation. Timescale ss09 not correct for Holocene (Johnsen et al., 1997).
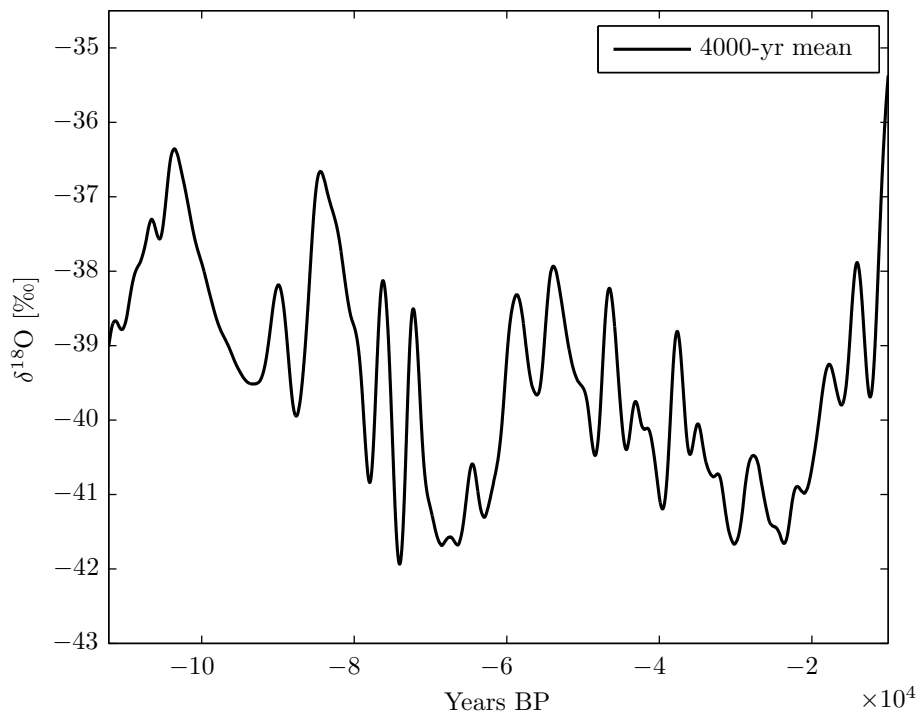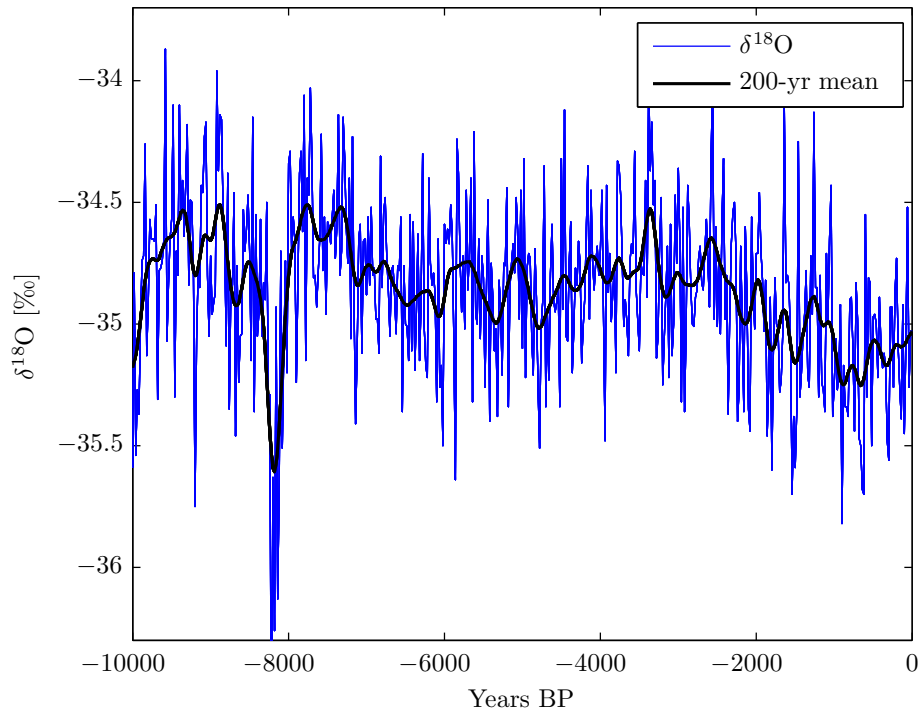
Figure 7: GRIP δ^{18}O-record with 200-yr and 4000-yr Gaussian low-pass filter.

C Code

C.1 Forward model

```matlab
1  function Tz = Tmodel(m)
2  global Tinit
3  global t
4
5  % Method 1
6  Qgeo = m(4);        % Geothermal heat flux (W/m^2)
7  k = m(5);
8
9  % Method 2
10 Qgeo= m(11);        % Geothermal heat flux (W/m^2)
11 k = m(12);
12
13 [Ts lambda] = Tsurf(m); % Surface temperatures
14
15 % From Dansgaard 93
16 zH = 3003.8;        % Ice thickness (m)
17 h = 1200;           % DJ kink height
18 fb = 0.15;          % D-J model bottom sliding ratio
19 Krock = 2.5;        % Thermal conductivity of rock W/(K*m)
20 rhorock = 2700;     % Density of rock kg/m^3
21 Crock=800;          % Specific heat capacity J/(K*kg)
22 dTdz_0= Qgeo/Krock; % Gradiant is found from the geothermal heat flux
23
24
25 % Height steps
26 zbed = -3000;
27 dz = 5;
28 z = zbed:dz:zH;          % -3000 to 3003 in steps of 5m.
29 Nz = max(size(z));       % Number of height steps
30 z0 = find(z == 0);       % The interface between ice and bedrock
31 He = zH-0.5*h*(1-fb);    % D-J model effective height
32
33
34 % Time
35 ddt = abs(t(1:end-1)-t(2:end))*31536000;
36 Nt = max(size(t));
37
38 % Initialize arrays
39 wz = zeros(Nz,1);
40 kz = zeros(Nz,1);
41 K = zeros(Nz,1);
42 rho = zeros(Nz,1);
43 C = zeros(Nz,1);
44 dKdz = zeros(Nz,1);
45
46 s = zeros(Nz,1);
47 r = zeros(Nz,1);
```

```matlab
48  a = zeros(Nz,1);
49  ad = zeros(Nz,1);
50  b = zeros(Nz,1);
51  bd = zeros(Nz,1);
52  c = zeros(Nz,1);
53  cd = zeros(Nz,1);
54  d = zeros(Nz,1);
55  Tz = zeros(Nz,Nt);
56
57
58  % Parameters in rock
59  kz(1:z0-1) = (Krock/(rhorock*Crock));   % Diffusivity [m^2/s]
60  wz(1:z0-1) = 0;                         % Vertical advection [m/s]
61
62  rho(1:z0-1) = rhorock;                  % Density [kg/m^3]
63  C(1:z0-1) = Crock;              % Specific heat capacity [J/(K*kg)]
64  K(1:z0-1) = Krock;             % Thermal conductivity [W/(K*m)]
65  dKdz(1:z0-1) = 0;              % Derivative of thermal conductivity
66
67
68  Tz(:,1) = Tinit;    % Initial temperature profile
69
70  % Begin time:
71
72  for ii = 1:Nt-1
73
74  % Vertical advection velocity
75  for jj = z0:Nz
76
77      if z(jj)>h            % D-J velocity
78          wz(jj)=-lambda(ii)*(z(jj)-0.5*h*(1-fb))/He;
79      else
80          wz(jj)=-lambda(ii)*((1-fb)*z(jj)^2/(2*h)+fb*z(jj))/He;
81      end
82
83  end
84
85  % Thermal conductivity and diffusivity
86  % Fukusako (1990):
87  rho(z0:Nz) = 917*(1-1.17e-4.*Tz(z0:Nz,ii));
88  % Cuffey & Paterson:
89  C(z0:Nz) = 152.5+7.122.*(Tz(z0:Nz,ii)+273.15);
90  K(z0:Nz) = 9.828*exp(-5.7e-3.*(Tz(z0:Nz,ii)+273.15));
91
92  if k == 1   % Paterson diffusivity
93  kz(z0:Nz) = (K(z0:Nz)./(rho(z0:Nz).*C(z0:Nz)));
94
95  elseif k == 2   % Fukusako (1990) diffusivity
96  kz(z0:Nz) = (0.002083286*Tz(z0:Nz).^2-0.271037908*Tz(z0:Nz)+36.962202916)/31536000;
97
98  elseif k == 3   % James (1968) diffusivity
99  kz(z0:Nz) = (8.43 - 0.101*Tz(z0:Nz))*1e-3*1e-4;
100 end
```

```matlab
101
102
103  % Derivative of thermal conductivity
104  dKdz(z0) = -(5.7e-3)*K(z0)*((1/dz)*(Tz(z0+1,ii)-Tz(z0,ii)))/(rho(z0)*C(z0));
105  dKdz(Nz) = -(5.7e-3)*K(Nz)*((1/dz)*(Tz(Nz,ii)-Tz(Nz-1,ii)))/(rho(z0)*C(z0));
106
107  dKdz(z0+1:Nz-1) = -(5.7e-3)*(K(z0+1:Nz-1)).*((1/(2*dz))*(Tz(z0+2:Nz,ii)-...
108                     Tz(z0:Nz-2,ii)))./(rho(z0+1:Nz-1).*C(z0+1:Nz-1));
109
110  % Crank-Nicolson method:
111
112  s = kz.*ddt(ii)/(2*dz^2);
113  r = (dKdz-wz).*ddt(ii)/(4*dz);
114
115
116  a([1 Nz]) = 0;
117  for j = 2:Nz-1
118      a(j) = r(j)-s(j);
119  end
120
121  b(1) = -1;
122  b(Nz) = 1;
123  for j = 2:Nz-1
124      b(j) = 1+2*s(j);
125  end
126
127  c(1) = 1;
128  c(Nz) = 0;
129  for j = 2:Nz-1
130      c(j) = -r(j)-s(j);
131  end
132
133  % Boundary conditions at interface
134  a(z0) = (-(K(z0-1)/(K(z0)+K(z0-1))));
135  b(z0) = 1;
136  c(z0) = (-(K(z0)/(K(z0)+K(z0-1))));
137
138  ad = -a;
139  ad(z0) = 0;
140
141  bd(1) = 0;
142  bd(Nz) = 1;
143  for j=2:Nz-1
144      bd(j) = 1-2*s(j);
145  end
146  bd(z0) = 0;
147
148  cd = -c;
149  cd(1) = 0;
150  cd(z0) = 0;
151
152
153  d(2:end-1) = ad(2:end-1).*Tz(1:end-2,ii) + bd(2:end-1).*Tz(2:end-1,ii) + ...
```

```
154                    cd(2:end−1).*Tz(3:end,ii);
155
156  d(1) = −dTdz_0*dz;
157  d(end) = Ts(ii);
158  d(z0) = 0;
159
160  Tz(:,ii+1) = TDMAsolver(a,b,c,d);
161  end
162
163  end
```

C.2   Surface temperatures

```
1   function [Ts lambda] = Tsurf(m)
2   % Method 1:
3   global d18oI
4   Ts = (m(1)+m(2).*d18oI+m(3).*d18oI.^2);
5
6   v =[−10.09; −0.653; −0.01042];
7   lambda = 0.23*exp(v(1)+v(2).*d18oI+v(3).*d18oI.^2)/31536000;
8
9   % Method 2:
10  global t
11  DJtime = [−112200 −25000 −10000 −8200 −7000 −5000 −2000 −1000 −400 0];
12  T0 = m(1:10);
13
14  Ts = interp1(DJtime,T0,t,'linear');
15  lambda = 0.23.*exp(0.0467.*(Ts+31.7)−0.000227.*(Ts+31.7).^2)/31536000;
16
17
18  end
```

C.3   Covariance matrix

```
1   clear all
2   clear global
3   global Cd
4   global Tinit
5   global d18oI
6   global t
7
8   dt = [1000 100 20];
9   t = [−112200:dt(1):−40000,−40000−dt(1):dt(2):−15000,−15000−dt(2):dt(3):0];
10
11  % Height:
12  zH = 3003.8;            % Ice thickness (m)
13  zbed = −3000;
14  dz = 5;
15  z = zbed:dz:zH;         % −3000 to 3003 in steps of 5m.
16  Nz = max(size(z));      % Number of height steps
```

```
17  z0 = find(z == 0);       % The interface between ice and bedrock
18
19  % Load GRIP borehole temperatures:
20  T = load('Data/sum95temp.txt');
21  T1 = [zH − T(:,1)' −3000];          % load height
22  T2 = [T(:,2)' 62];                  % load temp
23  Tinit = interp1(T1,T2,z(1:Nz),'linear','extrap')';
24
25
26  d18o = load('Data/grip−ss09sea−cl−20yr.txt');
27  d18oT = −d18o(end:−2:1,1);      % Dataset is not unique
28  d18oT = [d18oT;0];
29  d18oP = d18o(end:−2:1,2);       % Dataset is not unique
30  d18oP = [d18oP;−35.030000000000001];
31  d18oI = interp1(d18oT,d18oP,t,'linear');
32
33  % Covariance matrix of uncertainty in temperature
34  Csigma = diag(ones(Nz−z0+1,1)*5/1000);
35
36  % Covariance matrix of uncertainty in height
37  Cmc = nan(Nz−z0+1,Nz−z0+1,800);
38  for ii = 1:size(Cmc,3)
39  zz = (zH−z(z0:Nz)').*(1+randn.*0.001);
40  S = Tinit(z0:Nz)−interp1(zH−z,Tinit,zz,'linear','extrap');
41  Cmc(:,:,ii) = S*S';
42  end
43  C1 = mean(Cmc,3);
44
45  % The covariance matrix and the inverse
46  covD = Csigma+C1;
47  Cd = pinv(covD);
```

C.4   Loglikelihood

```
1  function logL = loglikelihood(m)
2  global Cd
3  global Tinit
4  % m = [...];
5  % S is residual/misfit. Fx: S = Tz(z0:Nz,end)−Tinit(z0:Nz);
6  % Cd is the global variable with uncertainties
7
8  Tz = Tmodel(m);
9
10 S = Tz(601:1201,end)−Tinit(601:1201);
11 logL = −0.5*S'*Cd*S;
12 end
```